Linear excitations in the $S=\frac{1}{2}$ ferromagnetic chain system $(C_6D_{11}ND_3)CuBr_3$ studied with neutron scattering

G. C. de Vries and E. Frikkee
Netherlands Energy Research Foundation ECN, P.O. Box 1, 1755 ZG Petten, The Netherlands

K. Kakurai* and M. Steiner
Hahn-Meitner Institut G.m.b.H., Glienickerstrasse 100, D-1000 Berlin 39, Federal Republic of Germany

B. Dorner
Institut Max von Laue–Paul Langevin, 156 X, 38042, Grenoble CEDEX, France

K. Kopinga and W. J. M. de Jonge
Eindhoven University of Technology, Department of Physics, P.O. Box 513, 5600 MB Eindhoven, The Netherlands
(Received 15 November 1988; revised manuscript received 5 July 1989)

The low-energy part of the dispersion relation of the intrachain magnons in the one-dimensional $S=\frac{1}{2}$ Heisenberg ferromagnet $(C_6D_{11}ND_3)CuBr_3$ has been determined with inelastic neutron scattering experiments. For reduced wave vectors q_c in the range $(0.07)2\pi/c \leq q_c \leq (0.25)2\pi/c$ and $T \approx 1.5$ K, well-defined excitations have been observed. The data can be described by linear spin-wave theory using the known values for the anisotropies and an isotropic part of the intrachain exchange interaction $J/k_B = 65.8 \pm 0.8$ K, which is in fair agreement with the value deduced recently from single-crystal heat-capacity measurements.

I. INTRODUCTION

The compound $(C_6H_{11}NH_3)CuBr_3$ (CHAB) is a very good representative of the one-dimensional (1D) $S=\frac{1}{2}$ ferromagnet. The nearest-neighbor intrachain exchange interaction in this system exceeds the interchain interactions by 3 orders of magnitude.[1] The weak interchain interactions lead to a 3D antiferromagnetic ordering below the Néel temperature $T_N = 1.5$ K. Heat-capacity measurements in the paramagnetic region have been interpreted on the basis of a 1D XY-Heisenberg model system with a 5% easy-plane anisotropy and $J/k_B = 55 \pm 5$ K.[1] Because of the existence of an easy plane, it is formally possible to transform the equation of motion of the magnetic moments in the chains in CHAB to a sine-Gordon equation, at least under certain approximations (classical spins confined to the XY plane, continuum limit, presence of a symmetry-breaking field).[2] The sine-Gordon equation has linear (spin waves) as well as nonlinear (kink solitons) solutions.

A satisfactory description of the observed magnetization for external fields within the XY plane was obtained by a model in which the linear excitations were treated quantum mechanically and the nonlinear excitations were treated by means of the classical sine-Gordon model.[3] The same model explains the qualitative behavior of the experimentally determined excess heat capacity $\Delta C = C(B) - C(B=0)$ and the experimental data on the nuclear spin-lattice relaxation (NSLR) time.[3] In view of these results we thought it worthwhile to obtain additional information on the static and dynamic properties of CHAB using neutron scattering techniques. We therefore synthesized deuterated single crystals (CHAB-D14). The details of the synthesis and the crystal structure have been published elsewhere.[4] The first part of our neutron scattering study[5] concerned the 3D ordering and the development of the magnetic correlations within the chains in zero field. A good overall description of the data has been obtained from transfer matrix calculations for a chain of classical spins using the appropriate spin Hamiltonian.

In this paper we report on the second part of our neutron scattering investigation, dealing with the linear excitations in CHAB. This study was, in part, motivated by the results of recent numerical calculations of ΔC in soliton-bearing chain systems like CHAB and $CsNiF_3$.[6–8] For CHAB, the results of these calculations show systematic deviations from the reported experimental data[9] which have been attributed to uncertainties in the values of the parameters in the spin Hamiltonian[6] or to the deviations of CHAB from ideal model behavior.[7] Since, on the other hand, the results of the various theoretical approaches are also, at present, still inconsistent in the experimentally relevant field and temperature region, an accurate estimate of the model parameters of CHAB seems of interest.

Inelastic neutron scattering experiments on the 1D $S=1$ easy-plane ferromagnet $CsNiF_3$ proved to be a successful technique to study not only the linear excitations,[10] but also the contribution of the nonlinear soliton excitations to the dynamic structure factor $S(\mathbf{Q},\omega)$.[11] In the case of CHAB, however, the low density of magnetic ions (a factor >3 smaller than in $CsNiF_3$), the low spin value ($S=\frac{1}{2}$), and the strong incoherent elastic scattering

(a factor >65 larger than in $CsNiF_3$ for the same sample volume), mainly due to the large number of deuterium atoms, precludes the identification of the solitons. We therefore confined ourselves to the study of the linear excitations.

The organization of this paper is as follows. After a short review of the crystallographic and magnetic properties of CHAB in Sec. II, the theory used in the interpretation of the data is briefly outlined in Sec. III. The data will be presented in Sec. IV, whereas the paper is concluded with a discussion in Sec. V.

II. CRYSTALLOGRAPHIC AND MAGNETIC PROPERTIES

The crystal structure of CHAB-D14 is an orthorhombic, space group $P2_12_12_1$, with four formula units per cell and cell dimensions $a=19.561$, $b=8.678$, and $c=6.381$ Å (at 54.5 K).[4] Powder x-ray measurements on the deuterated and the hydrogenated compounds did not reveal any significant change in the cell parameters and positions of the heavy atoms. Therefore, it was expected that the magnetic properties of CHAB would hardly change upon deuteration. This was confirmed by magnetization and ferromagnetic resonance (FMR) experiments on CHAB-H14 and CHAB-D14, which yielded results that were identical within experimental accuracy. The magnetic properties of the individual chains running along the crystallographic c axis can be described by the spin Hamiltonian

$$\mathcal{H}=-2\sum_i (S_i^x J^{xx} S_{i+1}^x + S_i^y J^{yy} S_{i+1}^y + S_i^z J^{zz} S_{i+1}^z) - \mu_B \mathbf{B}\cdot\vec{\mathbf{g}}\cdot\sum_i \mathbf{S}_i \ , \tag{1}$$

with $J^{xx}\geq J^{yy}>J^{zz}>0$. The intermediate y axis coincides with the crystallographic c axis, whereas the easy x axis is located in the ab plane at an angle φ from the b axis. Two symmetry-related types of chains are present with $\varphi=+25°$ and $\varphi=-25°$, respectively, φ being determined from FMR rotation diagrams.[12] Detailed FMR measurements on CHAB-H14 also yielded values for the anisotropy in the intrachain interaction which are given by $(J^{xx}-J)/k_B=0.92$ K, $(J^{yy}-J)/k_B=0.90$ K, and $(J^{zz}-J)/k_B=-1.82$ K. The isotropic part of the exchange interaction J is defined as $J=(J^{xx}+J^{yy}+J^{zz})/3$.[12] From zero-field heat-capacity measurements a value $J/k_B=55\pm5$ K has been inferred.[1] A 3D antiferromagnetic ordering occurs below $T_N=1.5$ K in CHAB-H14. The ordering temperature of the deuterated compound, $T_N=1.56$ K, is only slightly higher, which may be attributed to a small difference between the interchain interaction parameters J' of the two compounds. We will neglect these small interchain interactions throughout this paper.

III. LINEAR SPIN-WAVE THEORY

In this section we will briefly outline the derivation of the intrachain magnon dispersion relation for CHAB. The present inelastic neutron scattering experiments have been performed in a zero field and in an applied field along the crystallographic b axis. In the latter case the applied field is canted with respect to the preferred direction of the spins. In the zero field this direction is represented by the x axis in Hamiltonian (1), which is located in the ab plane at an angle $\varphi=\pm25°$ with the b axis. To describe the in-field situation we transform the Hamiltonian (1) to a new coordinate system $\tilde{x},\tilde{y},\tilde{z}$ as defined in Fig. 1, in which, according to the usual formalism, the $\tilde{z}$ axis represents the axis of quantization, i.e., the preferred direction of the spins in the presence of an applied field. The angle η between the x axis ($=\tilde{z}$ axis in the zero field) and the $\tilde{z}$ axis is field dependent. The Hamiltonian (1) in the $\tilde{x},\tilde{y},\tilde{z}$ system with $\mathbf{B}\|\mathbf{b}$ reads

$$\begin{aligned}\mathcal{H}=&-2\sum_i (S_i^{\tilde{x}} J^{\tilde{x}\tilde{x}} S_{i+1}^{\tilde{x}} + S_i^{\tilde{y}} J^{\tilde{y}\tilde{y}} S_{i+1}^{\tilde{y}} + S_i^{\tilde{z}} J^{\tilde{z}\tilde{z}} S_{i+1}^{\tilde{z}}) \\ &-g^b\mu_B B\cos(\varphi-\eta)\sum_i S_i^{\tilde{z}} \\ &-\sum_i (J^{zz}-J^{xx})(S_i^{\tilde{x}} S_{i+1}^{\tilde{z}} + S_i^{\tilde{z}} S_{i+1}^{\tilde{x}})\sin 2\eta \\ &-g^b\mu_B B\sin(\varphi-\eta)\sum_i S_i^{\tilde{x}} \ ,\end{aligned} \tag{2}$$

where

$$\begin{aligned} J^{\tilde{x}\tilde{x}} &= J^{zz}\cos^2\eta + J^{xx}\sin^2\eta \ , \\ J^{\tilde{y}\tilde{y}} &= J^{yy} \ , \\ J^{\tilde{z}\tilde{z}} &= J^{xx}\cos^2\eta + J^{zz}\sin^2\eta \ . \end{aligned} \tag{3}$$

Because of symmetry conditions, Eq. (2) is valid for both types of chains. For fields applied along the other crystallographic directions, Kopinga *et al.*[3] have derived similar expressions. Using the Holstein-Primakoff transformation[13,14] and retaining terms up to second order in the boson creation and annihilation operators, a_k^* and a_k, respectively, the Hamiltonian can be written as

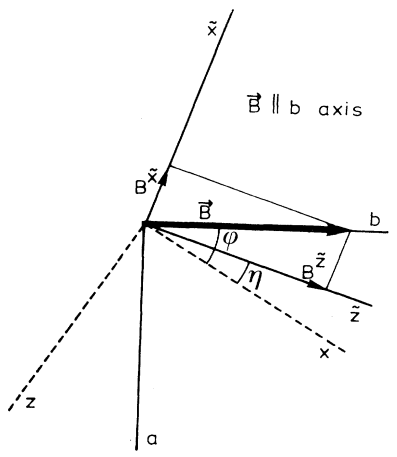

FIG. 1. Definition of the set of local axes $(\tilde{x},\tilde{y},\tilde{z})$ for an applied field along the b axis. The $\tilde{z}$ axis, i.e., the preferred direction of the spins, is located in the ab plane and coincides with the x axis for $B=0$ T. The $\tilde{y}$ axis coincides with the crystallographic c axis. The meaning of φ and η is explained in the text.

$$\mathcal{H}=\mathcal{H}_0+\mathcal{H}_{sw} ,$$

where

$$\mathcal{H}_0=-NS[2J^{\bar{z}\bar{z}}S+g^b\mu_B B\cos(\varphi-\eta)] ,$$
$$\mathcal{H}_{sw}=\sum_k[A_k a_k^* a_k+\tfrac{1}{2}B_k(a_k a_{-k}+a^*_{-k}a_k^*)] , \quad (4)$$

with

$$A_k=4J^{\bar{z}\bar{z}}S-2S(J^{\bar{x}\bar{x}}+J^{\bar{y}\bar{y}})\cos[k(c/2)]$$
$$+g^b\mu_B B\cos(\varphi-\eta) ,$$
$$B_k=-2S(J^{\bar{x}\bar{x}}-J^{\bar{y}\bar{y}})\cos[k(c/2)] . \quad (5)$$

The terms that are linear in a_k^* and a_k are absent in Eq. (4) as long as η satisfies the classical torque balance equation

$$2S(J^{zz}-J^{xx})\sin 2\eta+g^b\mu_B B\sin(\varphi-\eta)=0 . \quad (6)$$

In Eq. (5), $c/2$ equals the distance between neighboring spins, and $-2\pi/c\le k\le 2\pi/c$. The diagonalization of $\mathcal{H}_{sw}$ is accomplished by Bogoliubov transformation, yielding

$$\mathcal{H}_{sw}=\sum_k E(k)(\alpha_k^*\alpha_k+\tfrac{1}{2})-\tfrac{1}{2}\sum_k A_k , \quad (7)$$

with

$$E(k)=(A_k^2-B_k^2)^{1/2} . \quad (8)$$

$E(k)$ is the magnon dispersion relation used in the interpretation of our data, which will be presented in the next section.

IV. EXPERIMENTAL RESULTS

The spin-wave excitations in CHAB-D14 have been studied with inelastic neutron scattering. At the Risø National Laboratory, Denmark, we measured the low-energy part, $E<4$ meV, of the dispersion relation along the chains, checked the absence of dispersion perpendicular to the chains, and studied the behavior of the spin waves with reduced wave vector $q_c=0.135$ $(2\pi/c)$ as a function of temperature. In all these measurements, performed on the spectrometers TAS6 and TAS7, we used neutrons from the cold source. A first attempt to observe spin waves with energies larger than 4 meV at Risø's thermal beam instrument TAS3 was continued on the triple-axis spectrometer IN8 at the Institut Laue-Langevin, Grenoble, France. Table I contains a survey of the various experiments and important experimental parameters. The sample, a fully deuterated CHAB-D14 single crystal, gradually deteriorated upon the inevitable temperature cycles and by the chemical reaction reported in Ref. 4. The initial volume, approximately 1 cm^3, decreased in the subsequent measuring periods to $\sim$0.3 cm^3.

In Fig. 2 some typical sets of data, collected at temperatures just below and above the 3D ordering temperature, are depicted. The data have been corrected for the change of the resolution volume V_f ($\sim k_f^3\cot\Theta_A$) over

TABLE I. Experimental configurations; rlu is the reciprocal lattice unit and PG is pyrolytic graphite.

Spectrometer	Scattering plane	Monochromator, analyzer, collimation (min)	Neutron energy (meV)	Wave vector (Å^{-1})	Q (rlu)	ζ (rlu)	Temperature (K)	B‖b (T)	Crystal volume (cm^3)
TAS3 Risø	[110],c	60,PG,36,52,PG,66	$E_f=14.6$ $E_i=34.0$ $E_i=42.3$	$k_f=2.65$ $k_i=4.05$ $k_i=4.52$	various constant-**Q** scans		$\sim$1.5		$\sim$1
TAS6 Risø	[110],c	60,PG,36,81,PG,66	$E_i=4.710$	$k_i=1.508$	$-0.85,-0.85,\zeta$	0.070,0.085, 0.100,0.115 0.135,0.150, 0.170	1.4–1.5 1.4–1.5		$\sim$1
			$E_i=8.000$	$k_i=1.965$					
			$E_i=14.202$ $E_i=8.000$	$k_i=2.618$ $k_i=1.965$		0.21,0.25 0.135	1.9–2.0 1.5–50		
TAS7 Risø	[110],c	30,PG,60,81,PG,66	$E_f=4.000$	$k_f=1.389$	$\zeta,\zeta,0.085$	$-0.50,-i0.70,$ -0.85	1.5		2×0.25
IN8 Grenoble	a,c	45,PG,60,60,PG,60 45,Cu,60,60,PG,60	$E_f=8.000$ $E_f=14.68$ $E_f=34.83$	$k_f=1.965$ $k_f=2.662$ $k_f=4.100$	$-0.85,-0.85,\zeta$ $-2.4,0.0,0.2$ various constant-**Q** constant-E scans	0.135,0.170	1.6 1.6 1.6	0–6	2×0.15

the scan range.[15] The solid curves in Fig. 2 reflect the results of fits to the data with a Gaussian, the assumed resolution function, plus a constant background. All spin waves observed at $T \approx 1.5$ K ($\leq T_N$), with the exception of the spin wave with $q_c = 0.07$ $(2\pi/c)$, appear to have a resolution limited width. The effective width was calculated using a program based on the theory of Cooper and Nathans.[16] The corresponding spin-wave energies E_q are plotted in Fig. 3 as open circles. The integrated spin-wave intensities, scaled with respect to the integrated intensities of the observed elastic incoherent scattering, were found to be independent of the reduced wave vector q_c within a factor of 2, i.e., no systematic change in the intensities is observed.

The behavior of the spin waves at $q_c = 0.135$ $(2\pi/c)$ with $E_q \approx 1.2$ meV has been studied as a function of temperature. The spin-wave signal can be identified for temperatures up to 10 K. The results, corrected for V_f, are given in Fig. 4. In the fitting procedure used to derive the spin-wave energies E_q, based on a simple Gaussian plus a constant background, we left out those data points that are in the tail of the incoherent peak around $E = 0$. Especially in the scans at higher temperatures, this tail extends towards higher energies, which may give rise to an additional uncertainty in the results for E_q. In Fig. 5 the spin-wave energy E_q is shown as a function of temperature, where the error bars reflect the calculated 1σ statistical uncertainty in E_q. Although this uncertainty is quite large, the magnon energy appears to increase with increasing temperature. The broadening of the spin-wave signal observed above T_N may probably be attributed to the decrease of the correlation length ξ,[17] e.g., at 5 K (10 K) ξ amounts to ~ 6 spins (~ 2.5 spins),[5] whereas in the present experiments [with $q_c = 0.135$ $(2\pi/c)$] $q_c^{-1} \approx 2.4$

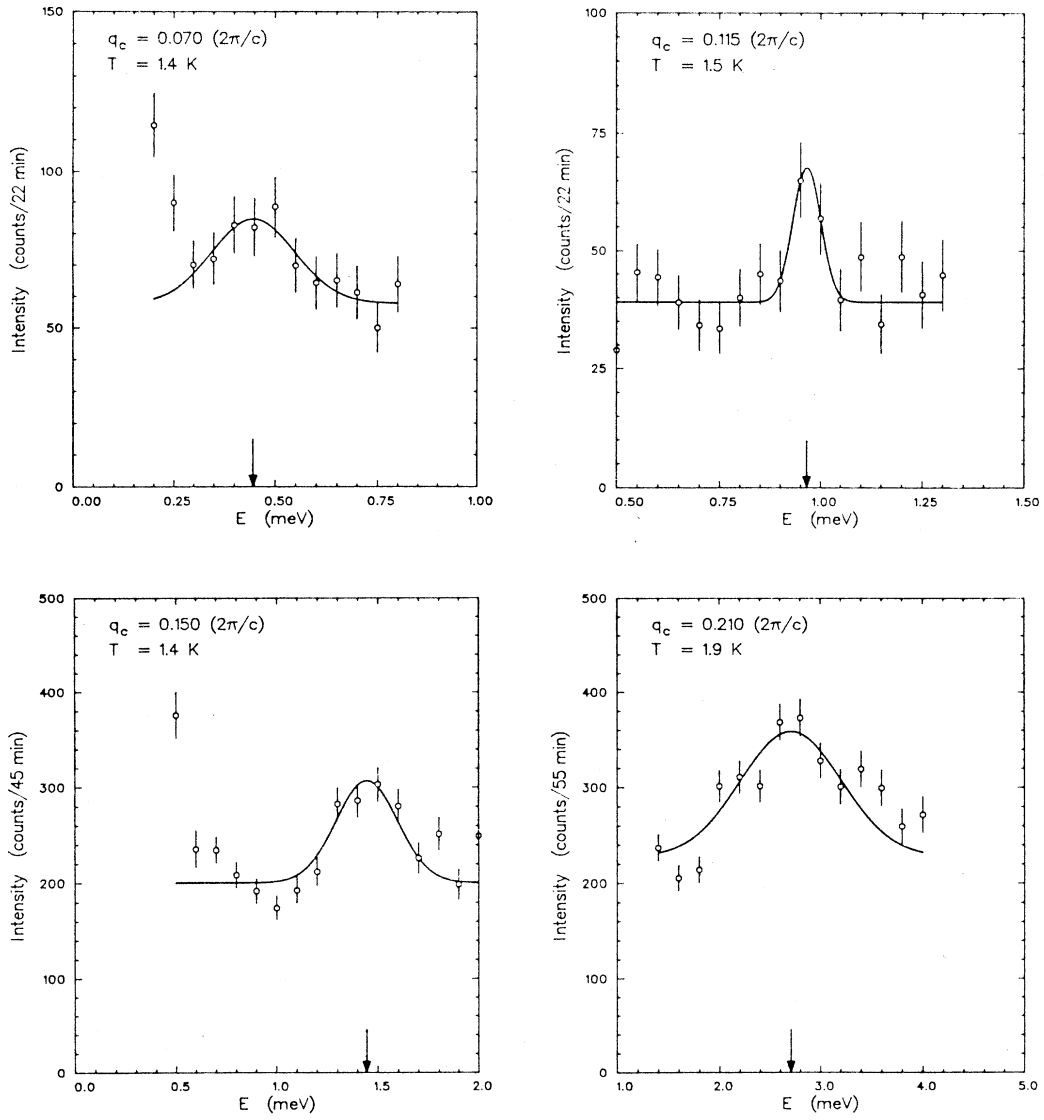

FIG. 2. Spin-wave scattering measured at TAS6 in constant-$\mathbf{Q} = (-0.85, -0.85, q_c)$ scans, with fixed incoming energies (see Table I). The solid curves are fits to the data which have been corrected for the change of the resolution volume V_f.

spins.

The dispersion perpendicular to the chain direction was investigated for the spin waves with $q_c=0.085$ $(2\pi/c)$ as a function of $q_{(110)}$ at $T=1.5$ K. The results are shown in the inset of Fig. 3. Within the experimental accuracy we do not observe any dispersion in the [110] direction, as expected for this 1D system. The crosses in Fig. 3 indicate the observed value of E_q, together with the results for two other spin-wave signals that have been measured at $T=1.6$ K, which is slightly higher than T_N. Figure 3 illustrates that there is no systematic difference between the spin-wave energies just above and below T_N. The same tendency is observed for the line shape; the signals remain resolution limited. These phenomena seem to be quite common to quasi-one-dimensional magnetic systems.[17,18]

As already mentioned, we tried to observe spin waves at higher energies by inelastic scattering measurements on the triple-axis spectrometer IN8. In order to separate the magnetic scattering from additional nonmagnetic inelastic scattering, the measurements were performed both in a zero field and in a magnetic field of 6 T, which is expected to produce a Zeeman shift of approximately $g\mu_B B \approx 0.7$ meV. The sample was oriented with the b axis along the (vertical) magnetic field. In that case, the effect of the applied field is identical for both types of chains. The ac plane is the scattering plane. The sample consisted of two aligned single crystals with a total volume of ~ 0.3 cm^3 The rocking curves of some Bragg reflections revealed that upon cooling down to 1.6 K, the two crystals were rotated with respect to each other around the ω axis ($=b$ axis) by 0.5°. In the actual experimental configurations, however, this small misalignment only resulted in differences in q_c or E_q that were smaller than the corresponding resolution.

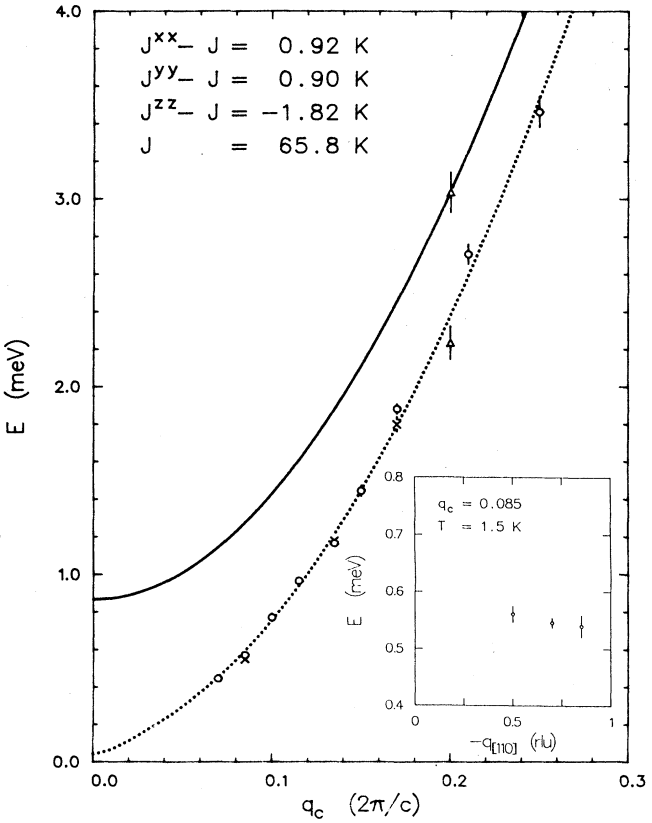

FIG. 3. The low-energy part of the intrachain spin-wave dispersion relation of CHAB-D14. The circles and crosses represent the zero-field measurements performed at TAS6 and TAS7, respectively. The two triangles denote the results of the zero-field and in-field ($B=6$ T along the b axis) measurements at IN8. The dotted curve is the result of a one-parameter fit to the zero-field data using the known anisotropies listed in the upper left corner. The fit yields $J/k_B=65.8\pm0.8$ K. The solid curve is the theoretical prediction for the dispersion in a magnetic field of 6 T parallel to the b axis. The inset shows the dispersion perpendicular to the chains.

The first measurements were done in the low-q_c range. Some results are shown in Fig. 6. Despite an unfavorable signal-to-background ratio, the field-induced shift of the magnon energy is well resolved. The triangles in Fig. 3 denote the corresponding magnon energies. Our attempts to observe spin waves with energies above 6 meV have been unsuccessful. We tried various experimental configurations where, on the basis of focusing considerations and the observed more or less constant scaling factor between the spin-wave intensity and the incoherent elastic intensity, a detectable spin-wave signal was expected. The reason for this negative result is not clear, especially since in a more or less comparable 1D ferromagnetic $S=\frac{1}{2}$ copper system, $CuCl_2\cdot DMSO$ (DMSO, dimethyl sulfoxide), Satija *et al.*[18] observed well-defined spin-wave signals in the entire q_c range above $q_c=0.25$ $(2\pi/c)$.

A one-parameter (J) fit including all zero-field data points, using expressions (5) and (8) with $B=0$ and anisotropy parameters given in Sec. II, yields a value of the isotropic part of the intrachain interaction $J/k_B=65.8\pm0.8$ K. The dotted line in Fig. 3 represents the corresponding theoretical prediction. The solid curve reflects the prediction for the same interaction parameters and a field of 6 T along the b axis. We used the value $g^b=2.06\pm0.04$ inferred from measurements of the saturation magnetization M_{sat}.[3] Under these experimental conditions the torque balance equation (6) yields, for the angle η, a value of 15.30°. From the results presented in Fig. 3 we conclude that the linear spin-wave theory outlined in Sec. III provides a very satisfactory description of the present inelastic neutron scattering data.

V. DISCUSSION

As already noted in the preceding section, the linear spin-wave theory describes the observed part of the dispersion relation of the in-chain magnons in CHAB very well. However, the inferred value $J/k_B=65.8\pm0.8$ K is 20% larger than the value $J/k_B=55\pm5$ K obtained from previous heat-capacity measurements.[1] We will return to this discrepancy in the last part of this section. First we comment on the approximations made in the analysis of the present neutron scattering data.

In the evaluation of the data we did not account for the

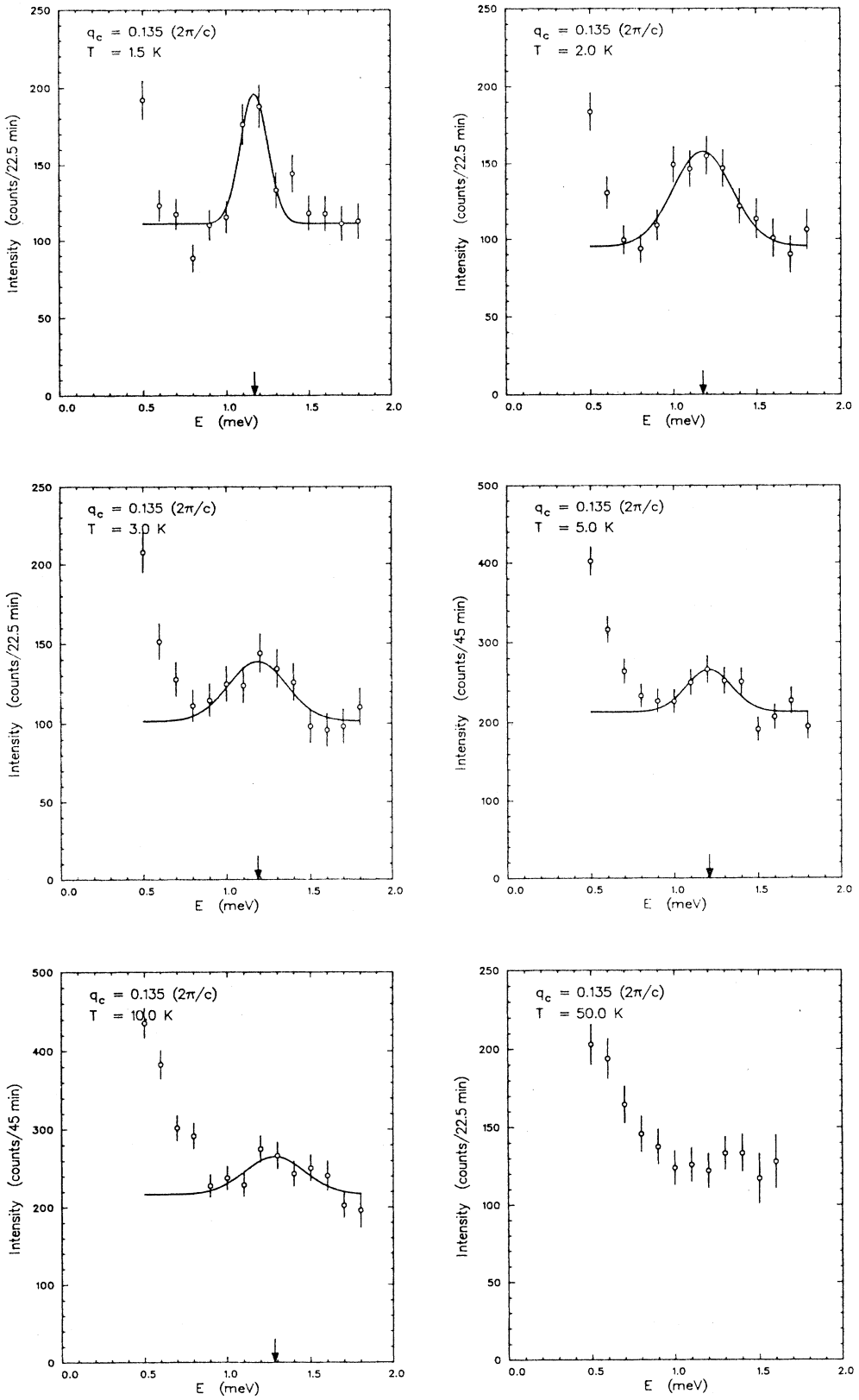

FIG. 4. Intensity profiles observed in constant-$\mathbf{Q}=(-0.85,-0.85,0.135)$ scans, as a function of temperature. $E_i=8.00$ meV, fixed. The solid curves are fits to the data which have been corrected for the change of the resolution volume V_f.

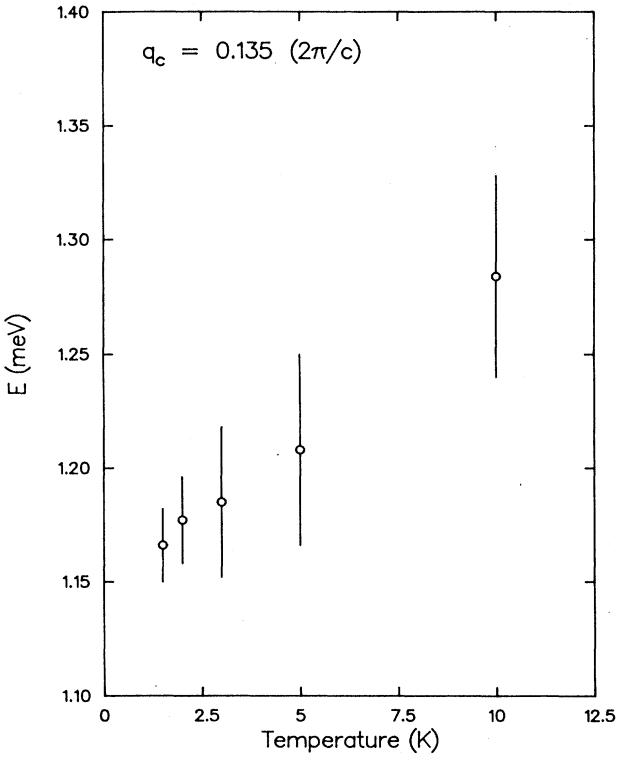

FIG. 5. Temperature dependence of the spin-wave energy at $q_c=0.135\,(2\pi/c)$.

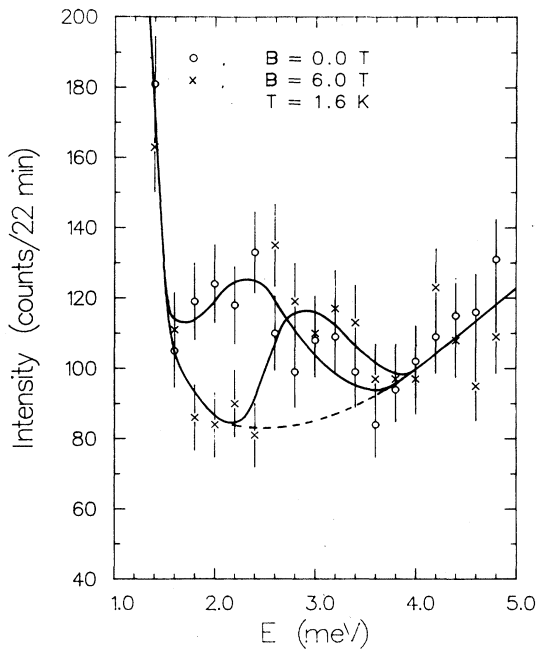

FIG. 6. Intensity profiles in the zero field and an applied field $B=6$ T along the b axis, measured at IN8 in constant-$\mathbf{Q}=(-2.4,0.0,0.2)$ scans. $E_f=14.68$ meV, fixed. The curves are guides to the eye.

different behavior of the spin components (S^x and S^y) within the easy plane and the spin component (S^z) along the hard axis. Such a difference has been predicted theoretically for a classical system with a large easy-plane anisotropy,[19,20] and is reflected by the behavior of the so-called in-plane correlation components (IPC), i.e., $\langle S_i^x(0)S_{i+p}^x(t)\rangle$ and $\langle S_i^y(0)S_{i+p}^y(t)\rangle$, and the out-of-plane correlation component (OPC), i.e., $\langle S_i^z(0)S_{i+p}^z(t)\rangle$. In the paramagnetic region the predicted IPC contribution to $S(\mathbf{Q},\omega)$ is broad, the full width at half maximum (FWHM) $\sim T$, and has a Lorentzian peak shape. The FWHM of the OPC contribution is predicted to be resolution limited. Because neutrons interact only with the spin components perpendicular to the momentum transfer $\mathbf{Q}$, it is, in principle, possible to separate the IPC and OPC contributions for a particular spin wave by carefully selecting the momentum transfer perpendicular to the chains. Using such a procedure, Steiner *et al.*[21] analyzed the IPC and OPC contributions in $CSNiF_3$, and found a behavior that quantitatively agreed with the predictions outlined above.

The statistics of the present data on CHAB is too poor to allow for a detailed analysis of the peak shape of the spin-wave signals. Moreover, such an analysis would be even more complicated than in the case of $CsNiF_3$ because of the presence of two types of chains, cf. Sec. II. In all scans on CHAB performed at $T>T_N$, we actually measured a superposition of IPC and OPC contributions. It is not clear to what extent the theoretical predictions for these contributions are applicable to CHAB ($S=\frac{1}{2}$, small easy-plane anisotropy). Since, however, the peak position of the IPC and OPC contributions is predicted to be the same, our analysis of the observed magnetic scattering with a single Gaussian will not affect the calculated spin-wave energy.

Both below T_N and in the paramagnetic region up to 1.6 K, i.e., $1.03T_N$, the observed widths of the spin-wave signals are resolution limited. This is the usual behavior for an ordered magnet where the linewidth reflects the relaxation rate of a collective excitation. In the paramagnetic region there is no long-range order and the linewidth is believed to be governed by the correlation length ξ.[17,18,21] The study of the temperature dependence of the magnetic scattering at $q_c=0.135\,(2\pi/c)$, cf. Figs. 4 and 5, reveals that well-defined signals exist at the zero field up to a temperature of 10 K, where the correlation length amounts to only 2.5 spins.[5] This indicates that the "naive" picture underlying the applicability of the Holstein-Primakoff transformation for a system in the paramagnetic region, i.e., the assumption that $\langle M\rangle/\langle M\rangle_{\rm sat}\simeq 1$, is rather oversimplified.

We finally return to the difference in the values for J/k_B obtained by the present neutron scattering experiments and the previous specific-heat measurements[1] on CHAB. For the analysis of the latter measurements, a theoretical model for the magnetic heat capacity C_M was used that was based on the extrapolation of numerical results for finite chains. Since the accuracy of these extrapolations strongly decreases at temperatures below 6 K, and at higher temperatures the experimental heat capacity is dominated by the lattice contribution C_L, the uncertainty in the inferred magnitude of J was rather large, as reflected by the reported value $J/k_B=55\pm5$ K. Recent-

ly, the zero-field heat-capacity data of CHAB, supplemented with measurements on a single crystal, have been reanalyzed using new and probably more accurate theoretical estimates for C_M.[7] This analysis (the details have been published separately[22,23]) yielded $J^{xx}/k_B = 63 \pm 3$ K, which is in good agreement with the value $J/k_B = 65.8 \pm 0.8$ K obtained from the present neutron scattering experiments. Given the small temperature dependence of the magnon energies suggested by the data presented in Fig. 5, we feel that the "zero-temperature" value $J/k_B = 65 \pm 2$ K provides a reliable starting point for a detailed quantitative comparison of various recent theoretical predictions for the thermodynamic properties of CHAB with the corresponding experimental data.

ACKNOWLEDGMENTS

The authors wish to thank the neutron scattering group of the Risø National Laboratory, Roskilde, Denmark, where a major part of the present experiments was carried out.

*Also at Risø National Laboratory, Roskilde, Denmark. Present address: Tohoku University, Sendai, Japan.

[1]K. Kopinga, A. M. C. Tinus, and W. J. M. de Jonge, Phys. Rev. B **25**, 4685 (1982).

[2]H. J. Mikeska, J. Phys. C **11**, L29 (1978).

[3]K. Kopinga, A. M. C. Tinus, W. J. M. de Jonge, and G. C. de Vries, Phys. Rev. B **36**, 5398 (1987).

[4]G. C. de Vries, R. B. Helmholdt, E. Frikkee, K. Kopinga, W. J. M. de Jonge, and E. F. Godefroi, J. Phys. Chem. Solids **48**, 803 (1987).

[5]K. Kopinga, W. J. M. de Jonge, M. Steiner, G. C. de Vries, and E. Frikkee, Phys. Rev. B **34**, 4826 (1986).

[6]G. M. Wysin and A. R. Bishop, Phys. Rev. B **34**, 3377 (1986).

[7]G. Kamieniarz and C. Vanderzande, Phys. Rev. B **35**, 3341 (1987).

[8]T. Delica, Phys. Rev. B **37**, 9879 (1988).

[9]A. M. C. Tinus, W. J. M. de Jonge, and K. Kopinga, Phys. Rev. B **32**, 3154 (1985).

[10]M. Steiner and J. K. Kjems, J. Phys. C **10**, 2665 (1977).

[11]M. Steiner, K. Kakurai, and J. K. Kjems, Z. Phys. B **53**, 117 (1983).

[12]A. C. Phaff, C. H. W. Swüste, W. J. M. de Jonge, R. Hoogerbeets, and A. J. van Duyneveldt, J. Phys. C **17**, 2583 (1984).

[13]T. Holstein and H. Primakoff, Phys. Rev. **58**, 1098 (1940).

[14]F. Keffer, *Handbuch der Physik,* edited by S. Flügge (Springer-Verlag, Berlin, 1966), Vol. 18/2, pp. 37–49.

[15]B. Dorner, Acta Crystallogr. A **28**, 319 (1972).

[16]M. J. Cooper and R. Nathans, Acta Crystallogr. **23**, 357 (1967).

[17]M. Steiner, J. Villain, and C. G. Windsor, Adv. Phys. **25**, 87 (1976).

[18]S. K. Satija, J. D. Axe, R. Gaura, R. Willett, and C. P. Landee, Phys. Rev. B **25**, 6855 (1982).

[19]J. Villain, J. Phys. C **6**, L97 (1973).

[20]J. Villain, J. Phys. (Paris) **35**, 27 (1974).

[21]M. Steiner, B. Dorner, and J. Villain, J. Phys. C **8**, 165 (1975).

[22]K. Kopinga, J. H. P. M. Emmen, G. C. de Vries, L. F. Lemmens, and G. Kamieniarz, J. Phys. (Paris) Colloq. **49**, C8-1451 (1988).

[23]K. Kopinga, T. Delica, and H. Leschke, Phys. Rev. B (to be published).